Journal of Solid State Chemistry 182 (2009) 3282–3288

Contents lists available at ScienceDirect

Journal of Solid State Chemistry

journal homepage: www.elsevier.com/locate/jssc

Low temperature molten-salt synthesis of nanocrystalline cubic Sr_2SbMnO_6

Antara Baral, K.B.R. Varma *

Materials Research Centre, Indian Institute of Science, Bangalore 560 012, India

ARTICLE INFO

Article history:
Received 6 May 2009
Received in revised form
4 September 2009
Accepted 8 September 2009
Available online 22 September 2009

Keywords:
Cubic phase
Molten-salt synthesis
Sulphate flux
Ceramic
Dielectric properties

ABSTRACT

Sr_2SbMnO_6 (SSM) powders were successfully synthesized at reasonably low temperatures via molten-salt synthesis (MSS) method using eutectic composition of 0.635 Li_2SO_4–0.365 Na_2SO_4 (flux). High-temperature cubic phase SSM was stabilized at room temperature by calcining the as-synthesized powders at 900 °C/10 h. The phase formation and morphology of these powders were characterized via X-ray powder diffraction and scanning electron microscopy, respectively. The SSM phase formation associated with ~60 nm sized crystallites was also confirmed by transmission electron microscopy. The activation energy associated with the particle growth was found to be 95 ± 5 kJ mol^{-1}. The dielectric constant of the tetragonal phase of the ceramic (fabricated using this cubic phase powder) with and without the flux (sulphates) has been monitored as a function of frequency (100 Hz–1 MHz) at room temperature. Internal barrier layer capacitance (IBLC) model was invoked to rationalize the dielectric properties.

1. Introduction

Materials possessing high dielectric constants (ε'_r) have been in increasing demand as these form important components in the area of microelectronics [1,2]. Lately, Sr_2SbMnO_6 (SSM) has generated considerable interest because of its large dielectric constant ($\sim 2 \times 10^5$ at 10 kHz, 360 K) [3]. SSM was reported to undergo a phase transition from ferroelectric (space group *I*4*mm*) to paraelectric (space group *I*4/*mmm*) at 450 K [4]. However, Cheah et al. [5] confirmed the space group to be *I*4/*m* by neutron powder diffraction (NPD) studies at room temperature. Indeed they could arrive at this space group by taking anti-site disorder of the Mn^{3+} and Sb^{5+} cations into account. The dielectric constant of SSM ceramic was reported to be frequency (100 Hz–10 MHz) and temperature (190–360 K) dependent [3]. In the oxide materials (which have cations that are likely to exist in more than one oxidation state depending on the preparation conditions etc.) associated with high dielectric constants, the contribution from extrinsic sources to the observed ε'_r is expected to be high, owing to their compositional heterogeneity and semiconducting nature.

Sr_2SbMnO_6 powders were prepared by the conventional solid-state reaction (SSR) route by heating the component carbonate/oxides at high temperatures (typically at 1350 °C for 45 h) [3] with a few intermediate grinding/heating cycles to achieve the maximum possible homogenization. However, this method yielded powders comprising rather coarse crystallites with a wide range of size distribution. Though the ceramics fabricated from these powders exhibited high dielectric constants, unfortunately their dielectric losses were also high which limit their use for possible capacitor and related applications. The dielectric loss however was known to decrease with decreasing crystallite size in electro-ceramics [6]. Therefore, we thought that it was worth synthesizing SSM powders comprising fine crystallites using technologically viable alternate routes.

Molten-salt synthesis (MSS) was known to be yet another method of technological interest for producing functional materials at finer scale at low temperatures [7,8]. Molten-salts as reaction media provide with an alternative to aqueous chemistry by offering the possibility to change the solubility and /or the reactivity of species. Because of the small diffusion distances in an intimate mix of the constituent oxides and relatively high mobility (1×10^{-5}–1×10^{-8} cm^2 s^{-1} compared to 1×10^{-18} cm^2 s^{-1} in the solid state) of the mass in the flux, the synthesis could be completed in a relatively short time and low temperatures [8]. The unstrained growing environment in the flux also benefits the crystals to attain their real morphological features according to their parent crystal structures [9]. The morphology is more distinguishable in the case of strongly anisotropic materials. It is believed that the morphologies are related to the surface and interface energies between the constituents and the salt, resulting in a tendency to minimize the energies by forming a specific morphology.

The environment for the development of specific morphology could be controlled by an appropriate choice of the salt. There are several requirements for the selection of salt in obtaining desirable powder characteristics. First, the melting point of salt

* Corresponding author. Tel.: +91 80 22932914; fax: +91 80 23600683.
E-mail address: kbrvarma@mrc.iisc.ernet.in (K.B.R. Varma).

0022-4596/$ - see front matter © 2009 Elsevier Inc. All rights reserved.
doi:10.1016/j.jssc.2009.09.006

should be low and it should not react with what is being synthesized. Further, the salt-solvent should possess sufficient aqueous solubility which can easily be removed by simple washing subsequent to the completion of the synthesis. A variety of molten-salt solvents such as alkali chlorides, sulfates, carbonates and hydroxides have been used as media of reaction for the constituent oxides which result in the formation of desired product at much lower temperatures than that of the conventional solid-state reaction route. We made systematic attempts to synthesize SSM fine powders using sulfate salts followed by the fabrication of ceramics and visualize their physical properties. The details pertaining to these studies are reported in the following sections.

2. Experimental

Stoichiometric mixture of AR grade $SrCO_3$, Sb_2O_3 and MnO_2 was thoroughly mixed with the eutectic composition of 0.635 Li_2SO_4–0.365 Na_2SO_4 [10] (30 mol% salts to oxide ratio) using a planetary ball mill for 4 h in propanol medium. The melting point of this composition is 594 °C. The mixed slurry was dried at 120 °C for 4 h for complete removal of propanol. The dried powder was subjected to a combined thermogravimetric and differential thermal analyses (TG-DTA) in the 300–900 °C temperature range at a heating rate of 5 °C/min to have a priori knowledge of the temperature for the required phase (SSM) formation.

To study the influence of reaction temperature on the phase formation, the mixture of the stoichiometric starting carbonate/oxides of SSM and 30 mol% sulfate was fired for 10 h for different temperatures (varying from 500 to 1000 °C). The heating rate was maintained at 15 °C min^{-1} and the cooling rate was at 25 °C min^{-1} till 300 °C and subsequently the mixture was furnace cooled to room temperature. The salts (flux) were ultrasonically washed using hot distilled water several times to ensure that the filtrate is free from SO_4^{-2} as confirmed by Ba $(NO_3)_2$ test. The obtained powders were fully dried at 120 °C for 4 h. The phase analysis of the resultant powder was carried out by X-ray powder diffraction (XRD) using Cu $K\alpha$ radiation (Philips PW1050/37). The grain size and its morphology were investigated using scanning electron microscope (SEM) (Quanta ESEM) and transmission electron microscope (TEM) (JEOL JEM 200CX). SSM powder was pressed into the pellets of 6 mm in diameter and 2 mm in thickness. These pellets were sintered in separate experiments at 1000, 1050 and 1075 °C for 16 h. XRD studies were subsequently performed on the sintered pellets which confirmed the tetragonal phase of the ceramics. The density of the samples was determined by the Archimedes method using xylene as the medium.

To make electrical property measurements, gold electrodes were sputtered on to the major faces of the sintered pellets and silver wires were glued on to the gold-coated surfaces using silver paste. Capacitance and dielectric loss measurements were carried out using the impedance gain phase analyzer (HP4194A) with a signal strength of 0.5 V_{rms}. The dielectric constant (ε'_r) was evaluated from the capacitance data by taking the electrode geometry of the sample into account using the formula

$$\varepsilon'_r = \frac{C \cdot t}{A\varepsilon_0}$$

where C is the capacitance of the sample, t is the thickness, A is the area of the electroded sample and ε_0 is the permittivity (8.854×10^{-12} F/m) of the free space.

3. Results and discussion

3.1. Thermal studies

The TG-DTA traces of thoroughly mixed starting carbonate/oxides of SSM in the 300–900 °C temperature range are shown in Fig. 1(a). The intense exothermic peak in DTA plot (Fig. 1(a)) around 515 °C is attributed to the transformation of Sb_2O_3 to Sb_2O_4 as reported in the literature [11]. The endothermic peak that is encountered around 760 °C corresponds to the decomposition of $SrCO_3$ accompanied by weight loss as confirmed by thermogravimetric analysis (Fig. 1(a)). Similar exothermic peak at 510 °C is noticed even for the starting mixture of carbonate/oxides of SSM mixed with 30 mol% sulfate (Fig. 1(b)). However, the endotherm for the decomposition of $SrCO_3$ is found to be at a lower temperature (680 °C) because of the influence of the flux (Fig. 1(b)). The exothermic peak that is incident around 870 °C in DTA (Fig. 1(b)) is ascribed to the formation of cubic SSM (as confirmed by the XRD studies, the details of which are given in the next paragraph) phase. The scheme of the chemical reaction associated with the formation of SSM could be written as:

$$2SrCO_3 + \frac{1}{2}Sb_2O_3 + MnO_2 + (\text{flux}) \xrightarrow{500\,^{\circ}C} SrCO_3 + \frac{1}{2}Sb_2O_4 + MnO_2 + (\text{flux})$$

(**a**) (**b**)

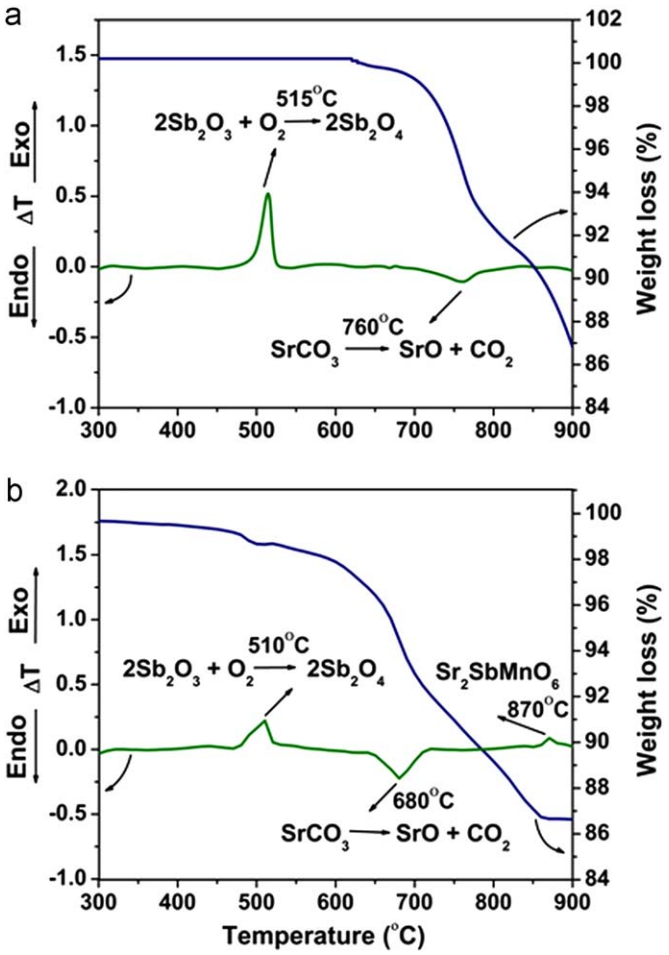

Fig. 1. TG-DTA curves for (a) stoichiometric mixture of starting carbonate/oxides of Sr_2SbMnO_6 (b) starting carbonate/oxides with 30 mol% of sulphate (0.635 Li_2SO_4–0.365 Na_2SO_4).

$$(\mathbf{b}) \xrightarrow{680\ ^\circ C} 2SrO + \frac{1}{2}Sb_2O_4 + MnO_2 + (\text{flux})$$

(**c**)

$$(\mathbf{c}) \xrightarrow{870\ ^\circ C} Sr_2SbMnO_6(\text{cubic}) + (\text{flux})$$

3.2. X-ray diffraction studies

The XRD patterns obtained for the calcined powders of $SrCO_3$, Sb_2O_3 and MnO_2 along with 30 mol% (0.635 Li_2SO_4–0.365 Na_2SO_4) flux at various temperatures (500–1000 °C/10 h) are shown in Fig. 2(a–g). The X-ray pattern obtained for the calcined powder at 500 °C/10 h consists of Bragg peaks corresponding to the constituent carbonate/oxides with no identifiable peak pertaining to the SSM phase. However, the one obtained for the calcined powder at 600 °C/10 h shows (Fig. 2(b)) a few Braggs peaks (marked as *), which could be assigned to SSM phase along with those corresponding to the starting carbonate/oxides. It is evident from Fig. 2(c–g) that the intensity as well as the number of peaks corresponding to SSM phase has increased with increasing calcination temperature indicating the enhancement in the formation of the volume fraction of SSM phase in the flux of mixed sulphate. It has been also noticed that with the increase in temperature the full-width at half-maximum (FWHM) of the diffraction peaks gradually decrease, suggesting an increase in the crystallite size (Fig. 2). The XRD pattern that is obtained for the sample (before washing) calcined at 900 °C confirms the cubic phase formation of SSM (Fig. 2(e)). It is also to be noted that the cubic phase transformed to tetragonal phase (Fig. 2(f) and (g)) on increasing the calcination temperature to 1000 °C. The Rietveld refinement of XRD obtained from the powders calcined at 1000 °C/10 h was carried out using FULLPROF software (Fig. 2h). Though the Rietveld refinement was carried out on various structural models like *I*4*mm*, *I*4/*m* and *I*4/*mcm*, comparatively less R_{wp} factor of 8% was achieved for the tetragonal crystal structure with space group *I*4/*mcm* and the lattice parameters, a=5.547 Å and c=8.089 Å. In the literature, Lufaso et al. [12] have suggested that the space group of fully disordered SSM is *I*4/*mcm*. Therefore, one can conclude that the compound prepared by molten-salt synthesis also adopts the same crystal structure due to the high degree of anti-site disorder.

Fig. 3(a) and (b) shows the XRD patterns recorded for the SSM powders prepared by MSS and solid-state reaction routes and were calcined at the same temperature, (900 °C/10 h). It is evident from Fig. 3(b) that this temperature is insufficient to obtain monophasic SSM using the solid-state reaction route. Fig. 3(a) depicts the XRD pattern recorded for the Sr_2SbMnO_6 powder (after washing) synthesized via MSS route. All the reflections could be indexed to a cubic cell associated with space group $Fm\bar{3}m$. The lattice parameter is refined using PROSZKI (powder diffraction data analysis software) which gives a=7.95(3) Å, and is in close agreement with that reported in the literature for high-temperature cubic phase of SSM [5]. The evolution of cubic SSM phase was monitored as a function of calcination temperature. The volume fraction (f) of the transformed SSM phase was determined on the basis of the XRD intensity ratio of the (2 2 0) peak for SSM phase and the intermediate oxide (Sb_2O_4 or SrO depending on the calcination temperatures) peak using the following equation [13]:

$$f = \frac{I(220)_{SSM}}{[I(220)_{SSM} + I_{Intermidiate\ Oxide}]} \quad (1)$$

Fig. 4 shows the variation in volume fraction of the SSM cubic phase as a function of the calcination temperature. The formation of SSM cubic phase is almost completed at 900 °C. An attempt has been made to estimate the crystallites size of the final cubic phase

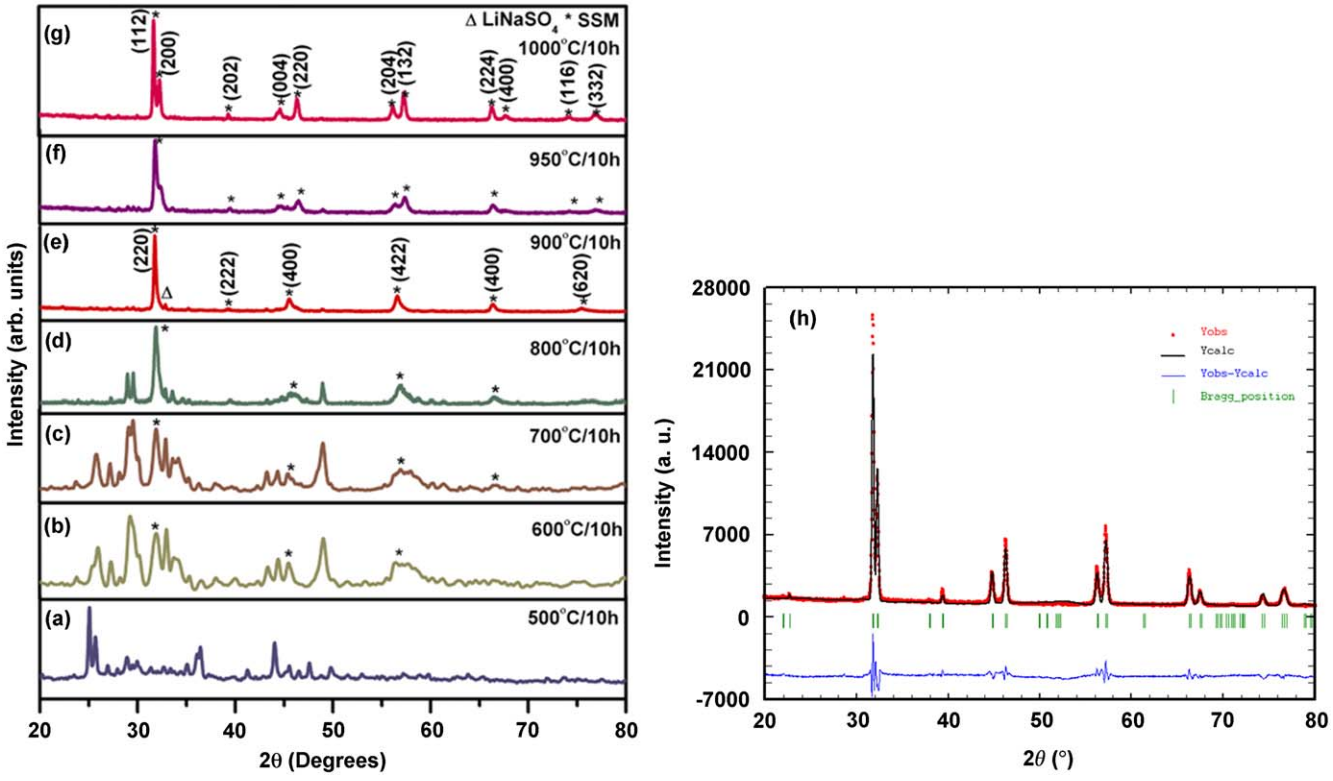

Fig. 2. (a–g) XRD patterns for the calcined (at different temperatures for 10 h) powders of the starting carbonate/oxides of Sr_2SbMnO_6 admixed with 30 mol% sulphate. (h) Observed and calculated X-ray patterns for the Rietveld refinement of Sr_2SbMnO_6. The bottom curve is the difference plot on the same intensity scale and the vertical markers show the positions of the space group allowed reflections.

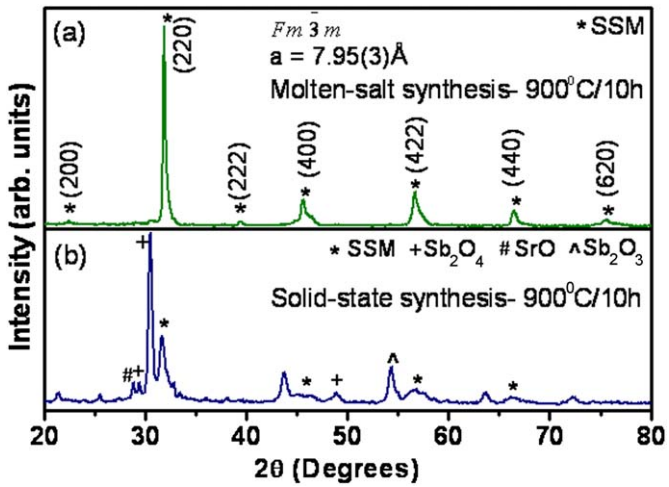

Fig. 3. XRD patterns obtained for (a) cubic phase Sr_2SbMnO_6 powders prepared by molten-salt (30 mol% sulphate) synthesis route and (b) the powders synthesized by solid-state synthesis route at 900 °C/10 h.

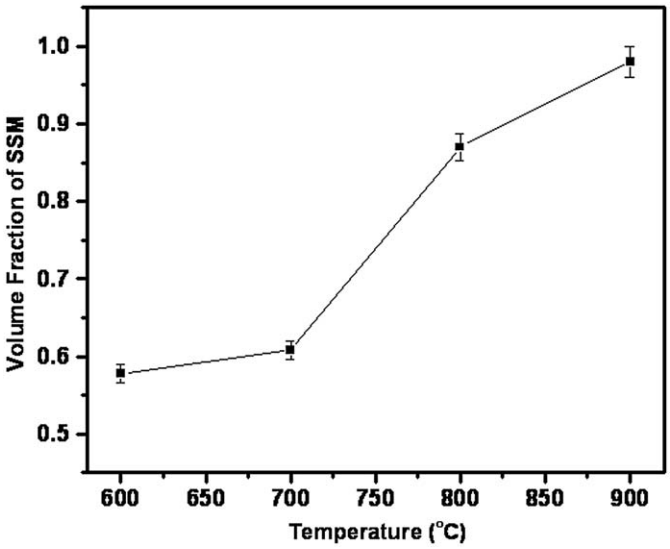

Fig. 4. Transformed volume fraction of the Sr_2SbMnO_6 phase in the sulphate flux (heated for 10 h) as a function of temperature. (Line is drawn as a guide to the eye.)

of SSM using X-ray line broadening technique [14]; the calculation was done using the SSM (2 2 0) diffraction line according to the Scherrer formula:

$$D = \frac{0.89\lambda}{\beta\cos\theta} \tag{2}$$

where D is the crystallite size; λ is the wavelength of the X-ray (Cu $K\alpha$, 1.5406 Å); θ is the diffraction angle and β is the corrected half-width given by

$$\beta^2 = \beta_m^2 - \beta_s^2 \tag{3}$$

where β_m is the measured full-width at half-maximum (FWHM) of SSM sample and β_s is the FWHM of a standard sample. The crystallite size that is obtained using the above formula is $\sim 55 \pm 6$ nm. This is corrected for possible errors in the measured β and θ for the cubic phase of SSM (900 °C/10 h).

3.3. Growth kinetic study

SSM powder was calcined at various temperatures (900–1025 °C) in order to make the crystal growth kinetic studies.

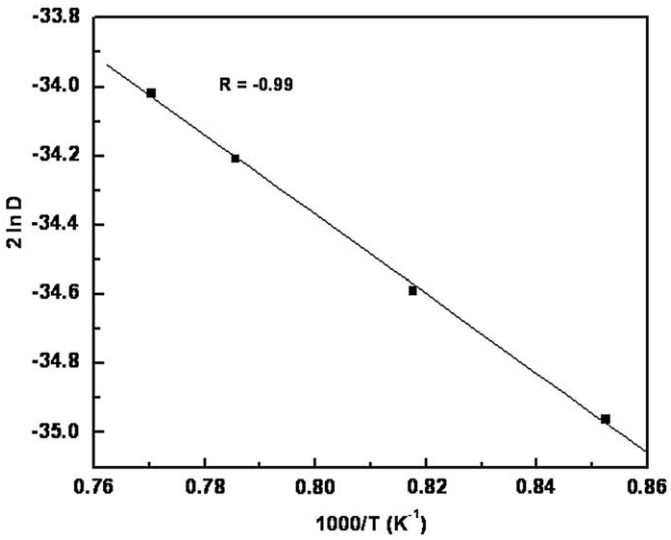

Fig. 5. Plot of $2\ln D$ versus $1/T$.

The crystallite size was determined using Scherrer formula based on the XRD data obtained for the powders calcined at different temperatures. The crystallite size is found to increase with increase in temperature. The particle growth behavior with temperature could be expressed as [15–18]

$$D^2 - D_0^2 = k(t - t_0)\exp\left(-\frac{E}{RT}\right) \tag{4}$$

where D is the average particle size at time t, D_0 is the initial particle size at time t_0, k is the rate constant, E is the activation energy associated with the particle growth, R is the gas constant and T is the calcination temperature. When the initial particle size, D_0, is small compared with the average particle size, D, at the time t, the factor D_0^2 can be neglected relative to D^2. The activation energy for the particle growth was calculated from the plot of $2\ln D$ versus $1/T$, which is shown in Fig. 5. The plot is found to be linear and fitted using the following equation:

$$2\ln D = \ln[k(t - t_o)] - \frac{E}{RT} \tag{5}$$

The activation energy that is obtained from the slope of the fitted line is $95 \pm 5\ \mathrm{kJ\,mol^{-1}}$ which is consistent with that reported in the case of the other oxides prepared by molten-salt synthesis route [19].

3.4. SEM and TEM studies

Fig. 6(a–c) shows the SEM micrographs of the stoichiometric mixture of oxides/carbonate heated at different temperatures. A change in the morphology of the constituent oxides has been found during the formation of SSM phase. Fig. 6(c) depicts the agglomerates of nanocrystals of cubic Sr_2SbMnO_6 powder obtained at 900 °C/10 h. One could also see the existence of individual nanocrystallites around the agglomerates. The morphology (acicular grains) of cubic SSM phase is different from that of the reactants as these have rod/plate-shaped particles. It is known that the solubility of the reactants in the molten-salt plays an important role in MSS which affects the size and morphology of the final phase.

Fig. 7 shows the TEM image of the water washed and dried SSM powder obtained by molten-salt synthesis at 900 °C/10 h (30 mol% of mixed sulphate was used as the flux). The average crystallite size was calculated from few images recorded at different locations of the sample and was found to be ~60 nm.

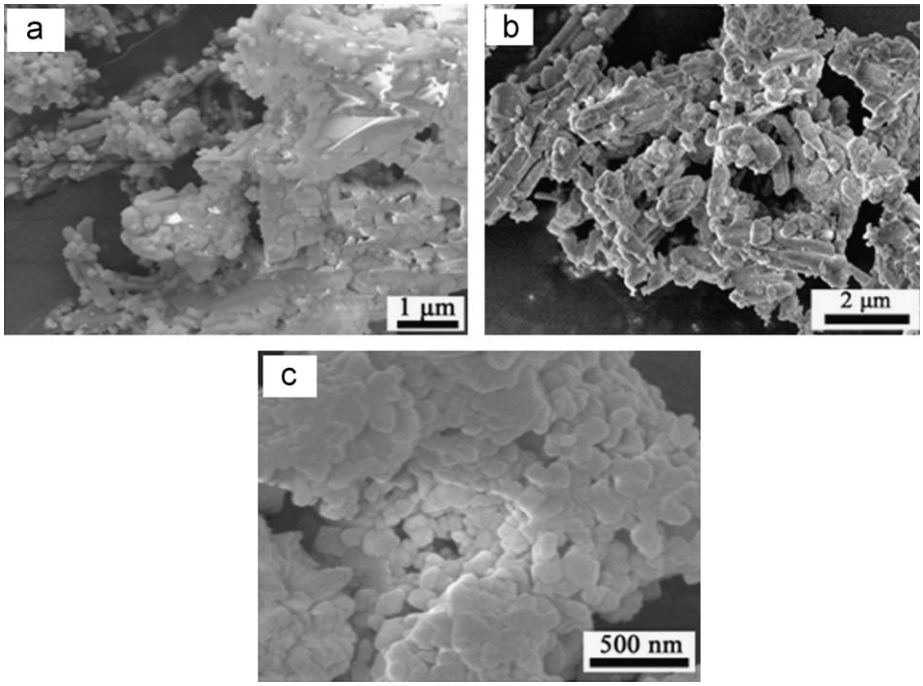

Fig. 6. SEM micrographs of the powders: (a) raw mixed carbonate/oxides and that heat treated at different temperatures (b) 500 °C/10 h and (c) 900 °C/10 h.

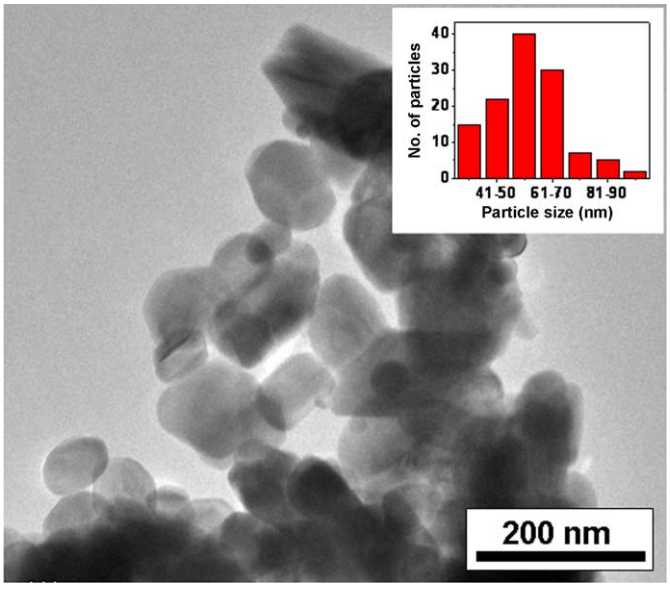

Fig. 7. TEM image of cubic Sr_2SbMnO_6 powder prepared by molten-salt synthesis at 900 °C/10 h. Inset shows the particle size distribution.

The histogram (given in the inset of Fig. 7) shows the size distribution of SSM crystallites. The crystallite size that is obtained using TEM is consistent with that obtained using the XRD studies.

In order to further elucidate the influence of salts (flux) on the sintering behavior, the green pellets of SSM (with salts and without salts) were sintered at various temperatures. For this purpose, Cubic SSM phase prepared using molten-salt synthesis at 900 °C/10 h was used. Fig. 8(a) and (b) shows the microstructural (SEM images) features of SSM ceramics (without salts i.e. after a thorough wash) sintered at 1000 and 1050 °C for 16 h. As expected, there is a decrease in porosity with the increase in sintering temperature.

The scanning electron microscopy were also carried out on the pellets (with and without salts) sintered at 1075 °C/16 h. Fig. 9(a) depicts the micrograph obtained for the pellet containing the salts. This micrograph reveals the distribution of a range of crystallite sizes while the one obtained without salts indicates the presence of uniformly grown grains associated with triple junctions (Fig. 9(b)). The XRD pattern recorded (Fig. 9(b′)) for this sintered pellet could be indexed to a tetragonal cell of SSM. The densities that were obtained for 1075 °C/16 h sintered pellets of SSM were 90% (with salts) and 96% (without salts).

3.5. Dielectric studies

Since, SSM ceramics fabricated from the powders obtained via the solid-state reaction route were known to exhibit high dielectric constants, we were curious to make these measurements on the ceramics obtained from the powders synthesized by MSS route. Fig. 10(a) and (b) shows the variation of the dielectric constant and the dielectric loss with frequency for the SSM pellets (with and without salts) which were sintered at 1075 °C/16 h. The sample that was sintered without the salts exhibits much higher dielectric constant (51938 ± 500 at 1 kHz, 300 K) than that of the samples sintered with the salt (6756 ± 60 at 1 kHz, 300 K). There is a strong low-frequency (100 Hz–10 kHz) dielectric dispersion in the ceramics containing no salts (Fig. 10(a)). The loss spectra (Fig. 10(b)) of SSM with salt indicate a single relaxation process whereas the loss spectrum of SSM without salt exhibits a unique relaxation behavior with two distinct peaks that can be attributed to the grain and grain boundary. This is actually a Maxwell–Wagner type relaxation where interfacial polarization arising from grain/grain boundary interface gives rise to high dielectric constant values [20]. The comparison further emphasises the role of microstructural modification in tuning the dielectric behavior of SSM.

The anomalously high dielectric constants at low frequency that are exhibited by the SSM ceramics make one to suspect that the underlying mechanism could be of extrinsic origin as a

consequence of the heterogeneity in the chemical composition of the grains. It is known especially in perovskite oxides that the electrical characteristics of the grains are different from that of the grain boundaries. Therefore exhibition of high dielectric constant has been attributed to the formation of the grain boundary internal barrier layer capacitance (IBLC) [21]. Though there could be different schools of thoughts about its origin. The thrust for adopting the IBLC model in SSM arises from its electrically heterogeneous nature in which the grains are conductive and the grain boundaries are resistive. One assumes that the grain and grain boundary form a two-layer capacitor with a thickness $\{d_g+d_{gb}\}$ where d_g and d_{gb} are the thicknesses of the grain and the

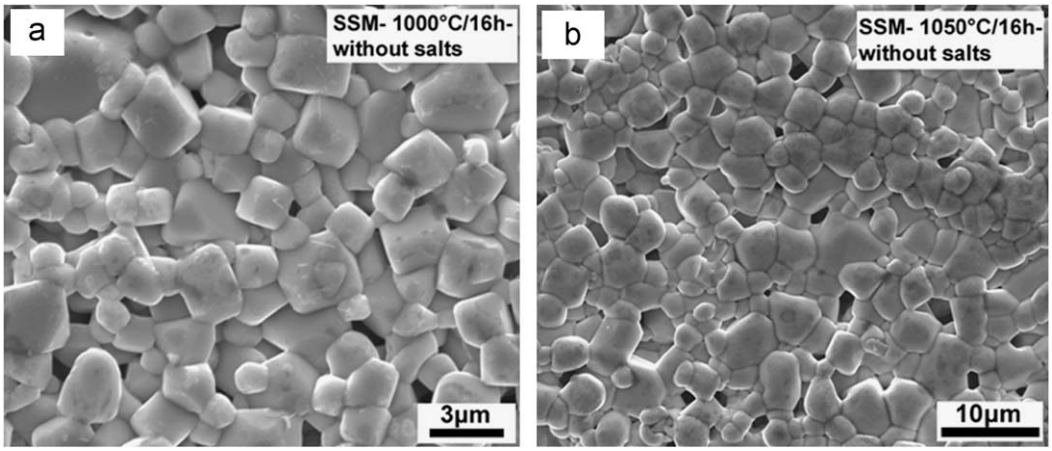

Fig. 8. SEM images of Sr_2SbMnO_6 pellets (without the salts) sintered at (a) 1000 °C and (b) 1050 °C for 16 h.

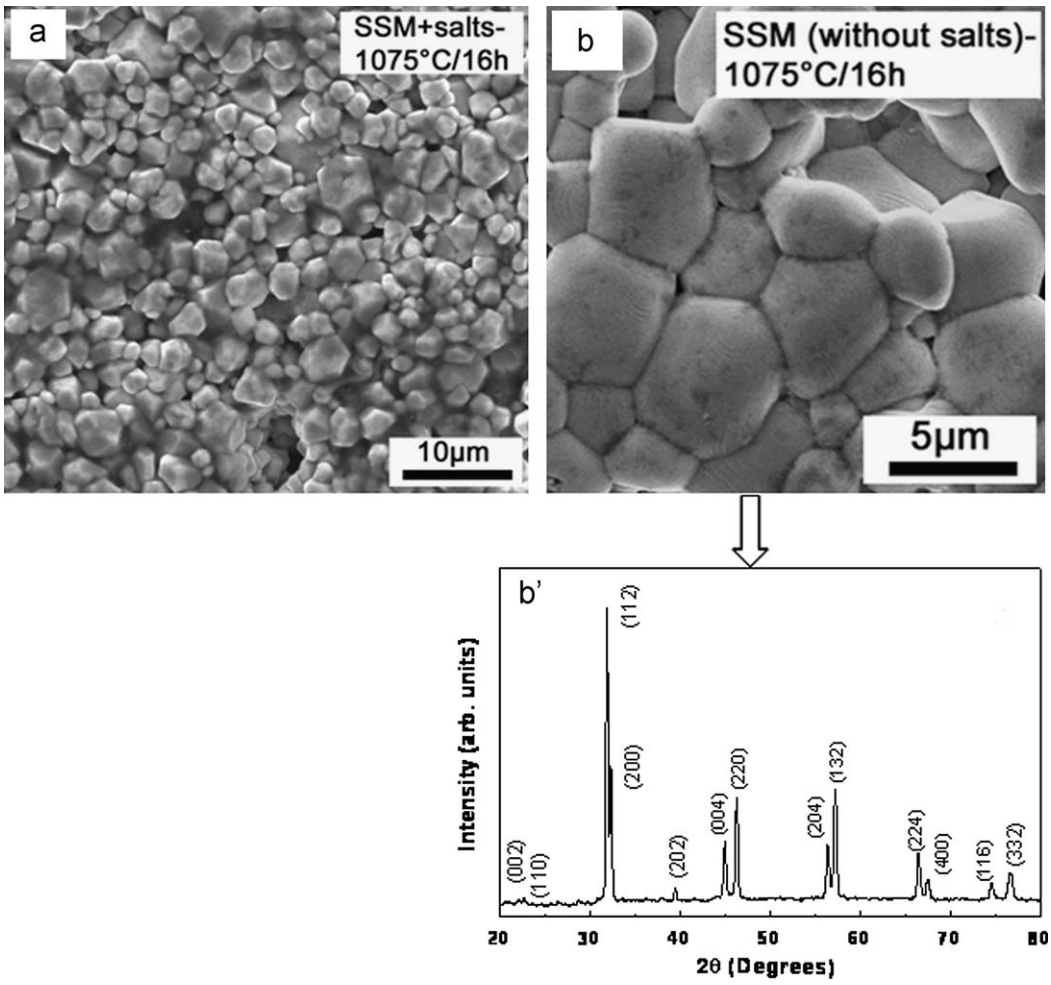

Fig. 9. SEM images of the 1075 °C/16 h sintered ceramics fabricated from Sr_2SbMnO_6 nanocrystalline powders (a) with salts (b) without salts (b′) corresponding X-ray powder diffraction pattern.

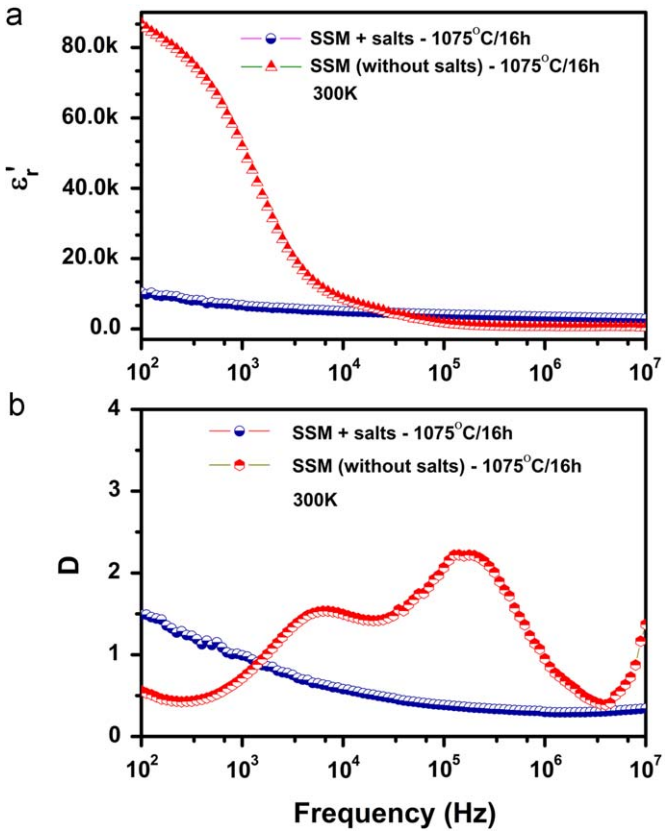

Fig. 10. Room temperature frequency dependent (a) dielectric constant (b) dielectric loss of Sr_2SbMnO_6 pellets sintered at 1075 °C for 16 h prepared by molten-salt synthesis routes (with and without the salts).

boundary layer, respectively. According to the barrier layer capacitance model, the effective dielectric constant is given by

$$\varepsilon'_s = \varepsilon_{gb}\left[\frac{(d_g + d_{gb})}{d_{gb}}\right] \quad (6)$$

where ε_{gb} is the dielectric constant of the grain boundary layer. In such a situation, even a small dielectric constant ε_{gb} can lead to a giant dielectric constant (ε'_s) if the ratio $(d_g+d_{gb})/d_{gb}$ is large. Hence, it is clear that ε'_s is highly dependent upon the microstructure and can therefore be maximized by enhancing the grain size (increasing d_g) or by thinning down the grain boundary, or by forming the grain boundary phase with high dielectric constant.

In the present case, the ceramic samples with no salts sintered at 1075 °C consist of nearly 2 times larger grains than that of salt containing samples. Therefore the usage of IBLC model is justified as large grains with higher density are expected to exhibit high dielectric constant.

The dielectric loss is lower for the ceramics fabricated using the powders obtained by MSS route as compared to that of the ceramics made via conventional solid-state reaction route [3]. The low dielectric loss is attributed to the reduction in the defect (mostly anion based) driven electrical conductivity associated with the SSM ceramics as these were sintered at relatively lower temperatures (1075 °C/16 h). When the complex oxides of the present kind are sintered at elevated temperatures (1350 °C/45 h) [3], as is the case with most oxides, nonstoichiometry with respect to the chemical composition is a serious problem which gives rise to high electrical conductivity vis-a-vis dielectric loss. When the ceramics are sintered at relatively low temperatures the conductivity problems associated with the non-stoichiometry are less effective as a result the dielectric loss is low.

Table 1
The dielectric constant and loss values (at room temperature) for Sr_2SbMnO_6 ceramics prepared by molten-salt synthesis routes with salts and without salts.

Dielectric properties	Frequency (Hz)	SSM with salts (300 K)	SSM without salts (300 K)
Dielectric constant (ε'_r)	1 kHz	6756 ± 60	51938 ± 500
Dielectric loss (D)	1 kHz	0.99	0.72

The dielectric constant and loss for the above-mentioned samples are reported in the Table 1. It is clear from the above studies that it is possible to fabricate SSM ceramics associated with high dielectric constant accompanied by relatively low dielectric loss using nanograined powders obtained by MSS route.

4. Conclusions

Fine powders (60 ± 6 nm) obtained by molten-salt (0.635 Li_2SO_4–0.365 Na_2SO_4) synthesis route on calcination at 900 °C/10 h yielded cubic phase Sr_2SbMnO_6. The structure transformed to the tetragonal by raising the calcination temperature to 1000 °C/10 h. Structural studies were carried out by the X-ray powder diffraction and transmission electron microscopy. The dielectric properties of the ceramics (containing no salts) sintered at 1075 °C/16 h exhibited anomalously high dielectric constants (51938 ± 500 at 1 kHz, 300 K) associated with low loss (0.72) as compared to that of the ceramics obtained from the powders containing the salt. An attempt has been made to rationalize this dielectric behaviour using IBLC model.

References

[1] S.M. Spearing, Acta Mater. 48 (2000) 179–196.
[2] G.H. Haertling, J.Am. Ceram. Soc. 82 (1999) 797–818.
[3] K. Majhi, B. Shri Prakash, K.B.R. Varma, J. Phys. D: Appl. Phys. 40 (2007) 7128–7135.
[4] M.C. Foster, R.M. Nielson, S.C. Abrahams, J. Appl. Phys. 82 (1997) 3076–3080.
[5] M. Elina Cheah, Paul J. Saines, Brendan J. Kennedy, J. Solid State Chem. 179 (2006) 1775–1781.
[6] K. Shantha, K.B.R. Varma, J. Am. Ceram. Soc. 83 (2000) 1122–1128.
[7] R Arendt, J. Solid State Chem. 8 (1973) 339–347.
[8] R Arendt, J.H. Rosolowski, J.W. Szymaszek, Mater. Res. Bull. 14 (1979) 703–709.
[9] C.C. Li, C.C. Chiu, S.B. Desu, J. Am. Ceram. Soc. 74 (1991) 42–47.
[10] A. Nacken, Neues Jahrb. Mineral. Ged. Beilage Bd. 24 (1910) 34.
[11] D.W. Zeng, C.S. Xie, B.L. Zhu, W.L. Song, Mater. Lett. 58 (2004) 312–315.
[12] Michael W. Lufaso, Patrick M. Woodward, Joshua Goldberger, J. Solid State Chem. 177 (2004) 1651–1659.
[13] S. Lee, et al., J. Mater. Res. 17 (2002) 2281–2285.
[14] P. Klug, L.E. Alexander, X-ray Diffraction procedure, Wiley-Interscience Publishing, New York, 1954, pp. 618–708.
[15] K.H. Yoon, Y.S. Cho, Y.W. Nam, D.H. Kang, J. Korean Ceram. Soc. 30 (1993) 543–548.
[16] J. Burke, Trans. Am. Inst. Min. Metall. Eng. 180 (1949) 73–77.
[17] S.D. Ramamurthi, Z. XU, D.A. Payne, J. Am. Ceram. Soc. 73 (1990) 2760–2763.
[18] J.R. Macewan, J. Am. Ceram. Soc. 45 (1962) 37–41.
[19] K.I. Hyun Yoon, Y.S. Cho, D.H. Kang, J. Mater. Sci. 33 (1998) 2977–2984.
[20] A.C. Couceiro, S.Y. Vilar, M.S. Andujar, J. Rivas, Prog. Solid State Chem. 35 (2007) 379–386.
[21] S. Sarkar, P.K. Jana, B.K. Chudhuri, Appl. Phys. Lett. 92 (2008) 022905-1–022905-3.